2025 European Conference on Computing in Construction

CIB W78 Conference on IT in Construction

Porto, Portugal
July 14-17, 2025

REBAR-TO-BIM: STEEL REINFORCEMENT RECONSTRUCTION FOR EXTENDED SCAN-TO-BIM WORKFLOWS

Fabian Kaufmann[1], Marius Schellen[1], Christian Glock[1], and Eric Hoeh[1,2]
[1]University of Kaiserslautern-Landau, Germany
[2]FK Horn construction Ltd., Kaiserslautern, Germany

Abstract

The creation of Building Information Modelling (BIM) models of existing structures has been widely researched, yet mainly covering visible components. For a structural assessment of concrete structures, the steel reinforcement contained in the component is as important as the outer dimensions. Ground penetrating radar (GPR) can be used for steel reinforcement imaging. This study will propose a methodology to align 3D reinforcement data with a BIM model, provide a 3D reconstruction of the rebar, and present it in an open BIM format. The method will be rigorously evaluated on the basis of two concrete test samples with known location and diameter of the reinforcement.

Introduction

Acquiring Building Information Modelling (BIM) models from existing structures is a crucial technology to apply BIM workflows to existing structures. Due to active research and development, there has been considerable advance in recent years, as the literature review of Schönfelder et al. (2023) reveals. However, most methods are limited to the acquisition of visible components ignoring embedded elements that provide the outer dimensions of the observed objects. Still, other aspects are crucial for a complete assessment of the structure. These aspects include obscured or cladded components, material information, and other properties. As concrete is the most widely used construction material (Friedlingstein, P., O'Sullivan, M., Jones, M. W., Andrew, R. M., Hauck, J., Olsen, A., Peters, G. P. et al., 2020), the steel reinforcement of concrete components needs specific attention to fully assess an existing structure.

To acquire 3D data as an input for scan-to-BIM, Light Detection and Ranging (LiDAR) and Structure from Motion (SfM) are used. Both technologies are available in efficient capture devices, even in hybrid approaches. The light waves used do not penetrate the surfaces of the objects. Thus, to scan steel reinforcement inside concrete components, other technologies must be applied. Among others, GPR is the most common technology. Relying on electromagnetic waves, any inhomogeneities in materials, e.g. a change in material from concrete to steel, cause a reflection that can be captured and combined to a 3D surface model of the reinforcement steel rods. This data can be used to reconstruct the cylindrical geometry of the reinforcement. Although there are other options, including ultrasonic sensors (Bittner et al., 2018) and large-scale computed tomography (Grzesiak et al., 2023) for internal concrete imaging, GPR is preferred in this study due to its ease of application and since large-scale computed tomography can only be applied to structural components extracted from existing buildings, not in situ to a complete structure.

This study aims to develop a method for 3D reconstruction of reinforcement steel members based on GPR scans. This includes scanning, GPR data processing, and reconstruction itself. Beyond mere reconstruction, an approach to align the GPR scan with a reference coordinate frame will be introduced. The method will be rigorously evaluated as follows. First, two concrete samples are designed and produced that contain steel reinforcement of varying arrangement and dimension. The diameter and location of the reinforcement are documented prior to the concrete being poured. After the concrete is poured and cure, both samples are scanned using Proceq GP 8000 and HILTI PS 1000 GPR scanners. After data processing, the reinforcement is reconstructed and the reconstruction is compared to the reference model.

In the civil engineering domain, the information retrieved is crucial to assess the structural behaviour, evaluate options for reuse of the entire structure, or preservation of components as a whole.

Related work

As our study aims to integrate 3D rebar reconstruction into a scan-to-BIM pipeline (Kaufmann et al., 2022), related work will be reviewed here in the field of structural component BIM reconstruction, as well as GPR-based rebar reconstruction.

Structural component BIM reconstruction

The approach to BIM wall object reconstruction presented by Bassier et al. (Bassier and Vergauwen, 2020) focusses on the extraction of IfcWallStandardCase objects from multi-storey building point clouds, including representations for curved and polyline walls, as well as a topology reconstruction framework to intersect or merge neighbouring wall objects. The proposed method comprises the identification of candidate connections based on

the k nearest neighbour, some restrictions including the avoidance of IfcSpace geometries, and distance thresholds, resulting in a set of valid connections. Bassier et al. (Bassier et al., 2020) expand their work and develop a comparative study on 2D and 3D wall reconstruction approaches. In this study, the 3D reconstruction approach comprises planar segmentation, an Support Vector Machine (SVM) classifier, a clustering per object and per floor, and a wall geometry reconstruction. The 2D approach includes a histogram-based storey segmentation, converting the points to a 2D point density raster image by projecting them onto the XY-plane, segmentation, clustering, and 3D wall points reconstruction. In the 3D method the 95 % confidence intervals is below +/- 5 cm for 88 % of the reconstructed walls, in the 2D method only 55 % are within the same error margin. Gankhuyag et al. (Gankhuyag and Han, 2021) propose a combination of 2D and 3D approaches with a two-step pre-processing procedure. After downsampling, the point cloud is upsampled to add missing points in the wall planes for better reconstruction accuracy. A 30 cm horizontal slice from below the ceiling is projected onto the XY-plane for an image-based wall line and junction detection. Subsequently, doors are detected by applying an iterative volumetric 3D search on the wall points. For all detected objects, IFC objects are created. The accuracy of the proposed method is above 90%. However, doors can only be detected when open.

Thomson et al. (Thomson and Boehm, 2015) propose a three-step approach to deliver wall and slab IFC objects. First, RANSAC (Fischler and Bolles, 1981) plane segmentation is applied with horizontal or vertical constraints to segment floor / ceiling and walls, respectively. Second, a Euclidean clustering with a planarity constraint is used to group planar patches of the same object. Finally, a convex-hull algorithm is used to retrieve the object's boundaries. Optionally, spatial reasoning is applied, e.g., to reject small walls, extend walls, or merge planes. As one of the few studies, Thomson et al. propose novel accuracy metrics, which are defined as the weighted sum of centroid deviation, normalised area error, and sine of angular deviation. Beyond building components such as walls, space objects are typically part of BIM models to represent rooms. To this end, Anagnostopoulos et al. (Anagnostopoulos et al., 2016a) propose a framework for wall reconstruction, object boundary extraction and correction, as well as space detection. The method relies on the object detection algorithm previously proposed in (Anagnostopoulos et al., 2016b) and reconstructs IfcWallStandardCase and IfcSpace objects. Space detection is limited to spaces fully encapsulated by walls. Most of the studies discussed propose to use 3D geometric or semantic segmentation as one of the first steps towards an as-built model. As their study focusses on the modelling and update of existing structural concrete work, Son et al. (Son and Kim, 2017) apply a material segmentation algorithm as the first step to identify all points related to structural concrete components. The scene is then further segmented, applying concavity and convexity criteria along the boundaries of the objects. The segmented patches are classified into columns and beam/girder using a SVM classifier. Beams and girders are further classified using connectivity relations. Finally, shapes are classified, geometric parameters are retrieved, and the model is delivered in an IFC compliant format. Kim and Kim (2021) propose to use a synthetic data-trained segmentation model to infer semantic labels, followed by Euclidean clustering to provide instance segmentation. After a planar patch segmentation, the vertices and edges are extracted by intersecting the planar patches per element. In case of incomplete scans, the dimension is inferred by referring to similar elements or default values. A graph network is used to model the relationships of the elements and a network update algorithm is applied to find missing relationships and to extend the elements according to related elements. In this study, synthetic data is used.

Rebar reconstruction and BIM integration

Although GPR devices are used for many applications in construction, there are only a few studies that seek to integrate these data into BIM combined with a BIM reconstruction of the scanned reinforcement.

Xiang et al. (2021) propose an automated framework to provide a 3D reinforcement reconstruction along with a reconstruction of the element the reinforcement is embedded in. Their study includes an approach to rebar recognition, a deep learning approach to classify the rebar and correlate it to types of structural elements, a method to translate the rebar to a BIM model, and a case study. Compared to our study, only line scans were performed in two perpendicular directions on the object. Although the evaluation in the study of Xiang et al. (2021) is limited to the rebar count and the detected depth, the evaluation proposed here includes the diameter and general precision of the reconstruction. In their study, the reference depth and count were obtained from the construction drawings, thus construction errors might not be considered in the reconstruction. Likewise, the average depth of the rebar was used in the rebar BIM model creation. In our study, we overcome this issue by (i) properly documenting the as-is position of the rebar while producing dedicated concrete test specimens and (ii) providing a dedicated reconstruction of each reinforcement bar, thus avoiding errors likely to occur by averaging parameters.

In a later study, Xiang et al. (2023) propose using labels and timestamps to correlate the GPR data and the as-built model. Compared to the previous study, IFC is used as BIM standard to maximize interoperability. However, the provided rebar BIM is still coarse as only line scans were performed to provide a 3D reconstruction yet not detecting any deviations in areas beyond the line scans. As a reference, Xiang et al. (2023) use the design drawings, yet suggesting to produce experimental concrete elements with full control of the rebar dimension and location, as is done in the proposed work here.

The research gaps can be identified as follows. Although

the topic of providing as-is BIMs based on spatial data is widely researched, the related work on integrating rebar reconstruction is limited. Based on the previous work discussed, the main gaps can be identified in performing rebar reconstruction based on 3D rebar data from GPR and a rigorous assessment of the retrieved diameter and location, and a concept for alignment based on machine-readable markers or labels. Although this study will provide approaches to overcome the first two research gaps, marker-based alignment will only be briefly discussed and is thus subject to future research.

Experimental setup and test elements

A key motivation for this study was to assess the accuracy of the scan and reconstruction. To achieve this, two dedicated test specimens were produced with known rebar dimensions and positions. The specimens have an outer dimension of 1.6 m x 1.6 m. The dimension reflects the fact that the HILTI GPR scanner uses a grid of 1.2 m x 1.2 m for 3D area scans. The Proceq GP 8000 scanner allows flexible adjustment of the grid in 0.1 m steps, making a 1.2 m x 1.2 m grid usable by both devices. A thickness of 30 cm was chosen as a realistic dimension of a slab in an office building. As in a real component, reinforcement is placed along both surfaces with coverage according to DIN EN 1992 1-1 (European Committee for Standardization, 2011), the standard applicable to concrete structures.

The first specimen containing rebar rods is shown in Figure 1. Rebar with diameters of 16 mm and 20 mm was used in both the top and bottom layers. To test scanning and reconstruction, overlapping rods are placed and spacers were installed to ensure a correct placement of the top and bottom layers. The reinforcement of the second test sample (see Figure 2) involves pre-fabricated rebar mats, a common choice for lower diameter rebars. In the upper layer, an R188A rebar mat was used with 6 mm rebar rods at a distance of 250 mm and 150 mm, respectively. In the bottom layer, a Q188A rebar mat with 6 mm rods at a distance of 150 mm was used. The chosen configurations represent typical bar configurations for slabs and walls, respectively. To align the BIM model of the reference rebar with the specimens after the concrete pour, a reference corner was carefully marked.

After the installation of the rebar, a 3D laser scan of the reinforcement was performed using a Leica MS 60. Along with 3D capture, the locations of the bar with reference to the shuttering were manually measured, deriving the coordinates of the end points of all the rebar. The rebar in the shuttering was placed and fixed as rigidly as possible to avoid movements during the concrete pour.

GPR data acquisition

After the concrete was poured, the test samples were prepared for GPR scanning. The preparation process includes the identification of the reference point and the attachment of the customised grid paper for GPR scanning as presented in Figure 3. The grid paper includes both a 10 cm

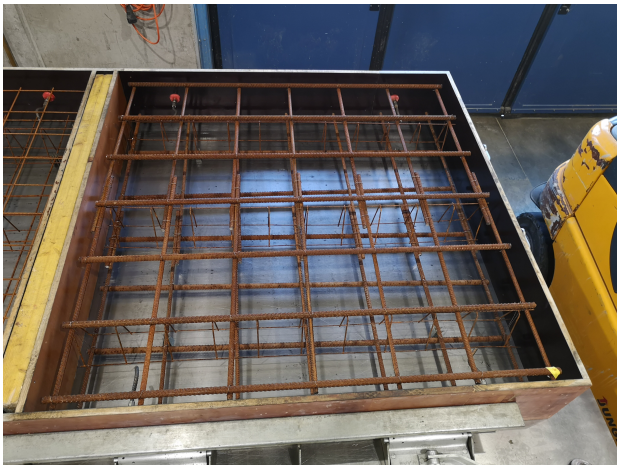

Figure 1: Test specimen 1 rebar rods before the concrete pour.

Figure 2: Test specimen 2 rebar mat before the concrete pour.

for the Proceq GP 8000 and a 15 cm grid for the HILTI PS 1000 GPR scanner. Depending on the scanner, the grid lines are numbered in a specific order.

The scan procedure follows the following steps: First, the workflow for an area scan is selected. The user interface, that is, the display on the HILTI PS 1000 and the Proceq GPR iPad App to which the Proceq GP 8000 is connected, then provides instructions in which order the lines of the grid should be followed. The devices are then moved slowly but steadily along the grid lines. As the devices measure the distance using sensors on the wheels, the end of the line is automatically detected, followed by a message which line to follow next. Depending on the device and the operator's routine, a scan takes approximately 10 to 15 minutes for the 1.2 x 1.2 m^2 grid.

After all lines have been traced, some parameters for the scan can be adjusted to optimise the GPR imaging. As the HILTI PS 1000 only offers very limited functionality to adjust the parameters, the adjustment will be explained along with the workflow of the Proceq GP 8000 and the Proceq GPR scanning app. The main parameter for scanning is the permittivity of the material scanned, in this case the permittivity of the concrete in which the reinforcement is

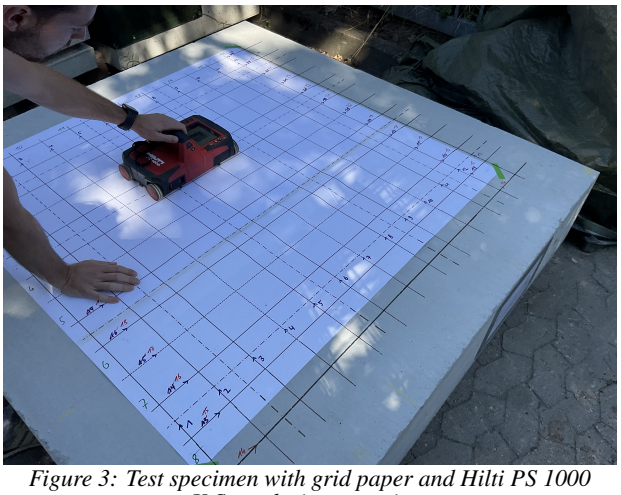

Figure 3: Test specimen with grid paper and Hilti PS 1000 X-Scan during scanning.

embedded. The permittivity of concrete has a range of approximately 4 to 14 depending on the moisture of the specimen. Thus, setting the permittivity correctly has a major impact on the results of the processed 3D data. In the Proceq GPR app, tags can be used to identify reinforcement or the back face of the specimen, thus facilitating a precise calculation of permittivity. In Figure 4, the back face tag can be seen along with the envelope curve. In terms of depth, the tag can be set by visually identifying the amplitude peak in the amplitude spectrum on the left-hand side. The envelope curve can then be visually adjusted. Setting the back face results in a permittivity of 12.1 for this specimen, a reasonable result.

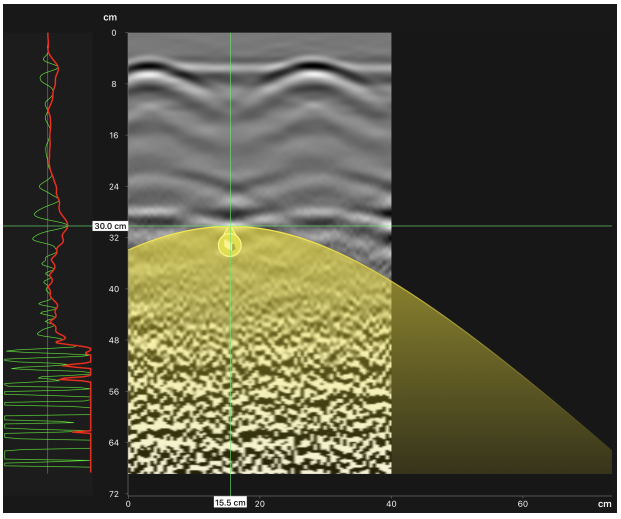

Figure 4: Tag of back face with envelope curve.

Based on the parameters set, different views and a 3D visualization of the reinforcement detected can be used to further refine the GPR data. However, a direct export of the 3D surface model from the Proceq GPR app is not possible. Thus, the data are exported in the SEG-Y format for further processing in the GPR Slice software [1]. This application offers a variety of tools for filtering, interpolating, and 3D visualisation of the data. A surface model is exported and used in 3D reconstruction.

Similarly, HILTI offers Profis detection software [2] to export a 3D surface model. However, the functionality is limited to a method to refine the mesh surface model followed by a 3D export. The main limitation here is that the upper layer of the reinforcement can be exported only, whereas GPR Slice offers full flexibility of processing and exporting the 3D data.

Although the workflows described are fairly different, a 3D surface model can be retrieved in a mesh representation that can then be used for 3D reconstruction of the reinforcement.

3D reinforcement reconstruction

Reference 3D model and data alignment

The reference model is created on the basis of two independent measurement campaigns. On the one hand, the position of each reinforcement rod is measured manually after the rebar cage had been produced. At each intersection, the rebar is fixed using wire; thus the reinforcement cage produced is rigid in itself. The coordinates measured manually and the diameter are then transferred into a table and exported as a CSV file. This file is used to automatically create 3D reinforcement objects using IfcOpenShell[3].

After installing the reinforcement in the shuttering, a laser scan was acquired using a Leica MS 60. The point cloud was used to mitigate any errors in the manual measurements and adjust the position with reference to the shuttering. The second step is critical, as the shuttering defines the outer surfaces and edges of the test specimen.

In a real-world application, the GPR scan must be aligned with the BIM model acquired through a scan-to-BIM pipeline. As suggested by Xiang et al. (2023), a common solution is to use markers as reference points. As the GPR scan requires a grid paper, a marker placed on the grid paper (see Figure 3) can be used to support the alignment of the GPR scan and the overall 3D data. As a second paradigm, the GPR scan could be aligned with the object's surface.

Although this is a practical solution, a different approach was used in this study. As a rebar reference model is available, the 3D rebar surface model is aligned with the reference model using the Iterative Closest Point (ICP) algorithm (Rusinkiewicz and Levoy, 2001). This eliminates errors resulting from the marker-based alignment procedure and demonstrates the maximum accuracy that could be obtained.

In Figure 5, the aligned 3D points retrieved from HILTI PS 1000 and the processing pipeline are shown together with the reference 3D model as a mesh representation. The reference BIM model provided in the IFC format is converted

[1] https://www.gpr-survey.com/

[2] https://www.hilti.de/content/hilti/E3/DE/de/engineering/software/detektion-detection-profis.html

[3] https://ifcopenshell.org/

into a mesh representation. CloudCompare (Girardeau-Montaut, 2020) was used to calculate the cloud-to-mesh distance, which is displayed as a colour scale.

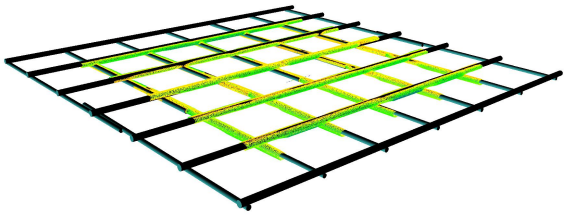

Figure 5: Test specimen 1 3D points with reference rebar model.

Cylinder fitting

The main task in 3D reconstruction is to approximate the set of unstructured 3D points by fitting geometric primitives. Reinforcement bars can be best approximated by cylinders. When a cylinder is fitted to a reinforcement bar in the point cloud, the parameters retrieved (axis, centre point, radius, length) can be subsequently used for automated BIM authoring. Primitive fitting inherently helps to avoid considering outliers and noise in the reconstruction step.

Kaiser et al. (2019) give a comprehensive overview of primitive fitting methods. One of the most popular approaches to primitive fitting is RANSAC shape detection. The basic principle is to randomly sample a number of points that define the respective geometric primitive. The deviations from the point set are calculated, and previously defined limits help to determine whether the fitted primitive can be accepted. RANSAC has a strict filtering side effect, which is beneficial to the accuracy of reconstruction. Beyond that, Kaiser et al. (2019) argue that RANSAC based methods are robust to outliers. The Hough transformation creates a collection area based on a set of parameters where similar geometric shapes meet. This area is divided into uniform sections, and each piece of data contributes to the voting for each geometric shape with which it aligns. The set of parameters that receives the most votes indicates the object that most accurately represents the given data. The main limitations are that the Hough transformation can be memory consuming and computationally expensive in the three-dimensional space, as the parameter space needs to be discretised. Similarly to RANSAC , in primitive-driven region-growing approaches, random seed points are initially selected. Adjacent points' features including colour, depth, or normal are then analysed to determine if the points observed can be assigned to a primitive. Compared to RANSAC, the filtering effect is less strict as there is no distance-to-primitive limit in region-growing approaches. Even slight curves in a plane primitive could be preserved in the segmented points. Kaiser et al. (2019) argue that region-growing methods are not robust when applied to incomplete data. This is intuitively evident, as the expansion of a region will terminate when no adjacent points are found, thus failing to retrieve the complete primitive and correct parameters.

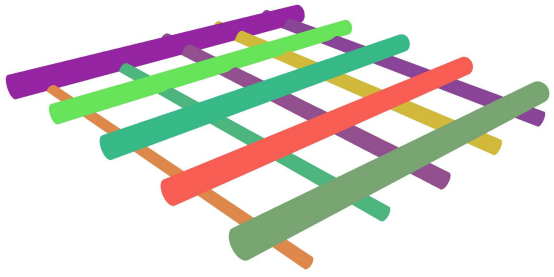

Figure 6: Test specimen 1 cylinder fitting from Proceq GP 8000 data.

Based on the study of Kaiser et al. (2019) and our experience in developing 3D reconstruction methods, efficient RANSAC as proposed by Schnabel et al. (2007) is selected as the primitive fitting algorithm for rebar reconstruction. Despite its advantages, setting the input parameters for a set of unseen data remains a challenge. However, only the correct input parameters allow the fitting to proceed and provide high accuracy. Thus, the input parameters, along with a strategy to set them, will be discussed. In this study, we will stick to the parameters' naming as it was chosen in CloudCompare Girardeau-Montaut (2020), a software that implements the efficient RANSAC algorithm.

The first input parameter to set is the minimum number of support points per primitive. In this case, the parameter name is indicative of what it controls, that is, the minimum number of points per primitive. By setting this value, primitives with a too small number of points will not be accepted during the iterative fitting process, resulting in an accurate number of primitives avoiding reconstruction artefacts. During our experiments, a formula could be derived empirically to estimate this parameter, where n_{min} denotes the minimum number of support points, n_{total} denotes the total number of points, and n_{bars} denotes the number of reinforcement bars suspected in the data.

$$n_{min} = 0.4 * \frac{n_{total}}{n_{bars}} \tag{1}$$

Obviously, n_{bars} might be difficult to estimate on unseen data. However, a rough estimate can still be found based on knowledge of structural engineering and the type of component. In any case, an estimate can be derived from a visual inspection of the unprocessed 3D GPR data.

The second parameter e denotes the maximum distance to the primitive, i.e. the maximum distance from the initial primitive that a point may have to be considered as an inlier. Setting e too low might result in multiple reconstructed cylinders of one real instance. An empirical

study on the influence of the parameter setting reveals that a value of e in the diameter range of the reinforcement bar yields the best results in the GPR data.

The third parameter to set is the sampling resolution b. This parameter controls the maximum distance of the primitive inliers. As mentioned above, RANSAC has a filtering effect. In terms of depth, this effect is controlled by setting b. A lower value of b causes the algorithm to exclude areas of lower point density from the primitive, or vice versa. Again, b can only be set based on an estimate of the density of the 3D data to be processed.

With the given parameters, the correct number of cylinders can be fitted to the data, as Figure 6 reveals. A rigorous evaluation of the reconstruction result will be presented in the Results evaluation section.

However, some errors in the reconstruction may still occur. Some examples and mitigation strategies will be presented in the following section.

Refinement

Despite carefully setting the RANSAC input parameters, reconstruction errors may still occur (see Figure 7). Two main issues were commonly encountered. Either two adjacent cylinders have been fitted that share approximately the same centre axis or overlapping cylinders have been fitted, where one can be considered an artifact. Erroneous cylinders can in both cases be identified by comparing the centre axes' direction and the euclidean distance of the end points. Although a straightforward option could be to just merge adjacent cylinders with the same centre line or just removing the smaller intersecting cylinder considered as an artefact. However, for a more accurate reconstruction, an efficient RANSAC cylinder fitting with changed parameters is again performed to better fit a cylinder.

Results evaluation

In line with the scope of this study, the results were evaluated on two criteria. First, the diameter recovered during reconstruction will be compared with the actual diameter. The general accuracy of the reconstruction is evaluated by calculating the distance between the reconstructed bar and the reference bar. As the reconstruction has been performed on the HILTI PS 1000 and Proceq GP 8000 data sets, both reconstructions can be compared in terms of diameter and overall accuracy. Note that per test specimen, the average diameter is reported on two layers of reinforcement and for type of reinforcement bar individually. For the reinforcement mat, the layers and distance of the individual bars are reported to assess whether the distance of the bars causes a significant effect. The notation, e.g., 6/15 cm, denotes the bar diameter in millimetres and the distance of the bars in centimetres.

On a general level, the diameter reconstructed with a minimum deviation of 1.88 mm (Specimen 1, Layer 1 $\varnothing$ 20 mm) $is far from accurate (see Table 1). To this end, providing an accurate diameter is challenging due to technical restrictions of GPR. C$

The second evaluation was performed by calculating the Euclidean distance of the reconstructed and reference ge-

Table 1: Evaluation of the as-is and reconstructed diameter. The reconstructed diameter is presented as the mean of all reinforcement bars present.

Specimen 1 reinforcement bars			
Layer	$\varnothing$ [mm]	Hilti [mm]	Proceq [mm]
1	16	21.79	59.53
1	20	21.88	66.64
2	16	26.91	43.10
2	20	27.99	58.85
Specimen 2 reinforcement mat			
Layer	$\varnothing$ [mm]	Hilti [mm]	Proceq [mm]
1	6/15cm	22.35	36.98
1	6/25cm	25.90	43.72
2	6/15cm	19.32	36.09
2	6/15cm	20.90	29.85

Table 2: Evaluation of the average distance of the reconstructed rebar and the reference rebar geometry.

Specimen 1 reinforcement bars		
Hilti PS 1000		
Layer	Mean [mm]	Std. dev. [mm]
1	3.88	5.72
2	5.96	6.56
Proceq GP 8000		
Layer	Mean [mm]	Std. dev. [mm]
1	24.10	13.21
2	19.61	11.17
Specimen 2 reinforcement mat		
Hilti PS 1000		
Layer	Mean [mm]	Std. dev. [mm]
1	9.59	5.51
2	8.15	3.97
Proceq GP 8000		
Layer	Mean [mm]	Std. dev. [mm]
1	19.02	9.12
2	15.17	9.88

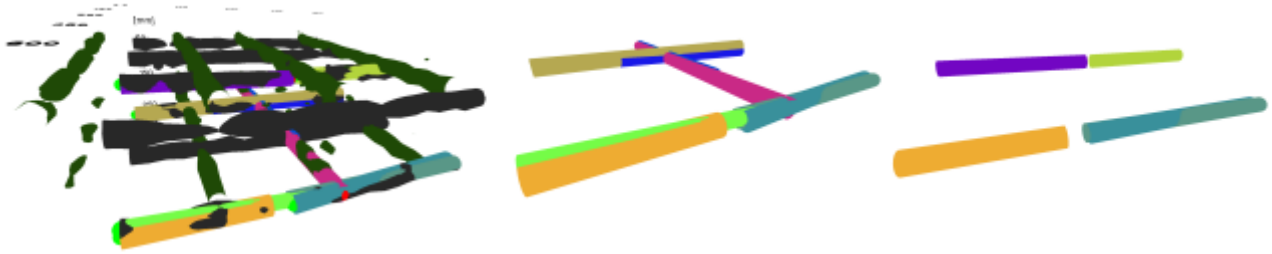

Figure 7: Reconstruction errors. Left: raw data with reconstructed cylinders. Middle: intersecting cylinders. Right: adjacent equi-directional cylinders.

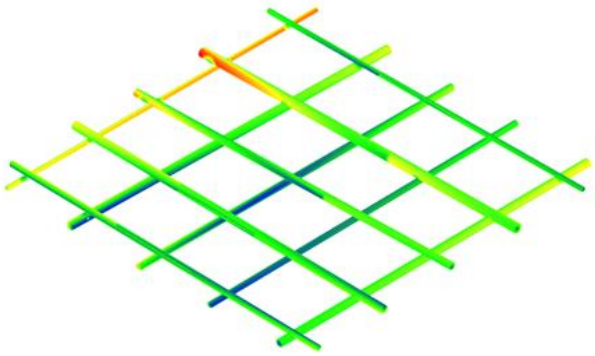

Figure 8: Cloud-to-mesh distance of reference and reconstructed reinforcement bars. Test Specimen 1, Hilti PS 1000 X scan.

ometry (see Table 2). To this end, a point cloud was subsampled on the reconstructed geometry that was then used to calculate the euclidean distance point-wise. Generally, the mean distance of the reference and reconstructed reinforcement bars obtained from the HILTI PS 1000 data is considerably lower than that of the Proceq GP 8000 data (see Table 2). This is consistent with the fact that the average diameter of the reconstruction of the Proceq data is considerably larger (see Table 1).

Discussion and conclusions

The mean distance of the HILTI PS 1000 reconstruction clearly reveals that the reconstruction accuracy is usable to deliver a BIM model of the bar with a sufficient accuracy. A visual inspection (see Figure 8) reveals that the deviation is the result of slight misalignments and an overestimation of the diameter when comparing the reconstructed and reference geometry. This leads to the conclusion that the data obtained from the GPR can be used to reconstruct the location of the reinforcement bars inside the concrete samples but are not accurate in terms of diameter. The Proceq GP 8000's diameter accuracy is less accurate, the location, however, can be considered appropriate. To this end, the device manufacturers do not specify a diameter accuracy achievable and even state that GPR scanning with the devices used will not be accurate in terms of the diameter retrieved but can indicate the position of the rebar.

In this study, the reconstructed rebar was aligned with the reference model. This is impractical in a real-world application as no reference rebar model might be available. In a future study, a marker-based alignment shall thus be implemented and tested to evaluate the accuracy of reconstruction in a more realistic scenario. The approach considered would incorporate marker systems on the grid paper providing a reference of the grid and thus the 3D reconstructed data with reference to the marker positions. By conventional surveying techniques, the markers' positions would then be acquired with reference to the BIM coordinate frame. This alignment method is applicable to newly reconstructed or existing BIM models.

To accurately determine the diameter of the reinforcement bars in the concrete specimen, two options can be considered. A non-destructive option is to use dedicated devices to measure the diameter of the bar and the concrete coverage, for example, the Proceq Profometer [4] or other comparable devices. As a destructive option, the rebar can be uncovered, revealing the diameter of the rebar.

In the civil engineering domain, any information is critical to perform structural assessments, e.g., for reuse and alteration or the preservation of components as a whole. To this end, even the location of the rebar is helpful. Providing this information aligned with a BIM model has the potential to really increase the efficiency of structural health assessment. However, our method cannot still accurately provide the concrete coverage and diameter of the rebar, which will be subject to future research. This aligns with the need to test the method in practical application. Compared to manual rebar modelling, it would be interesting to evaluate the potential savings in time and cost by further highlighting the practicality of the approach. To further enhance practicality, the size of the scanned area can be further increased with custom grid papers when using the Proceq device.

Declaration of generative AI and AI-assisted technologies in the writing process

During the preparation of this work, the author(s) used ChatGPT to improve the spelling, grammar, and style of the text snippets provided to the model. Likewise, Writefull as integrated into Overleaf was used to improve the

[4] https://www.screeningeagle.com/de/products/profometer-pm8000

language and readability of the text. After using this tool/service, the authors reviewed and edited the content as needed and take full responsibility for the content of the published article.

Acknowledgements

This work is part of the HumanTech project and has received funding from the European Union under Grant Agreement No. 101058236. HumanTech is a three-year project that started on 1 June 2022 and terminates on 31 May 2025.

References

Anagnostopoulos, I., Belsky, M., and Brilakis, I. (2016a). Object boundaries and room detection in as-is bim models from point cloud data. In Proceedings of the 16th International Conference on Computing in Civil and Building Engineering, Osaka, Japan, pages 6–8.

Anagnostopoulos, I., Pătrăucean, V., Brilakis, I., and Vela, P. (2016b). Detection of walls, floors, and ceilings in point cloud data. In Perdomo-Rivera, J. L., Gonzáles-Quevedo, A., Del Puerto, C. L., Maldonado-Fortunet, F., and Molina-Bas, O. I., editors, Construction Research Congress 2016, pages 2302–2311, Reston, VA. American Society of Civil Engineers.

Bassier, M. and Vergauwen, M. (2020). Unsupervised reconstruction of building information modeling wall objects from point cloud data. Automation in Construction, 120:103338.

Bassier, M., Yousefzadeh, M., and Vergauwen, M. (2020). Comparison of 2d and 3d wall reconstruction algorithms from point cloud data for as-built bim. Journal of Information Technology in Construction, 25:173–192.

Bittner, J. A., Spalvier, A., and Popovics, J. S. (2018). Internal imaging of concrete elements: Ultrasonic technology is developing as a practical nondestructive inspection tool. Concrete International, pages 57–63.

European Committee for Standardization, editor (2011). EN 1992-1-1 Eurocode 2: Design of concrete structures - Part 1-1: General rules and rules for buildings, Brussels. CEN.

Fischler, M. A. and Bolles, R. C. (1981). Random sample consensus. Communications of the ACM, 24(6):381–395.

Friedlingstein, P., O'Sullivan, M., Jones, M. W., Andrew, R. M., Hauck, J., Olsen, A., Peters, G. P. et al. (2020). Global carbon budget 2020. Earth System Science Data, 12(4):3269–3340.

Gankhuyag, U. and Han, J.-H. (2021). Automatic bim indoor modelling from unstructured point clouds using a convolutional neural network. Intelligent Automation & Soft Computing, 28(1):133–152.

Girardeau-Montaut, D. (2020). Cloudcompare: 3d point cloud and mesh processing software.

Grzesiak, S., Barisin, T., Schladitz, K., and Pahn, M. (2023). Analysis of the bond behavior of a gfrp rebar in concrete by in-situ 3d imaging test. Materials and Structures, 56(9).

Kaiser, A., Ybanez Zepeda, J. A., and Boubekeur, T. (2019). A survey of simple geometric primitives detection methods for captured 3d data. Computer Graphics Forum, 38(1):167–196.

Kaufmann, F., Glock, C., and Tschickardt, T. (2022). Scalebim: Introducing a scalable modular framework to transfer point clouds into semantically rich building information models. In Proceedings of the 2022 European Conference on Computing in Construction, Computing in Construction. University of Turin.

Kim, H. and Kim, C. (2021). 3d as-built modeling from incomplete point clouds using connectivity relations. Automation in Construction, 130:103855.

Rusinkiewicz, S. and Levoy, M. (28 May-1 June 2001). Efficient variants of the icp algorithm. In Proceedings Third International Conference on 3-D Digital Imaging and Modeling, pages 145–152. IEEE Comput. Soc.

Schnabel, R., Wahl, R., and Klein, R. (2007). Efficient ransac for point-cloud shape detection. Computer Graphics Forum, 26(2):214–226.

Schönfelder, P., Aziz, A., Faltin, B., and König, M. (2023). Automating the retrospective generation of as-is bim models using machine learning. Automation in Construction, 152:104937.

Son, H. and Kim, C. (2017). Semantic as-built 3d modeling of structural elements of buildings based on local concavity and convexity. Advanced Engineering Informatics, 34(6):114–124.

Thomson, C. and Boehm, J. (2015). Automatic geometry generation from point clouds for bim. Remote Sensing, 7(9):11753–11775.

Xiang, Z., Ou, G., and Rashidi, A. (2023). An integrated framework for bim development of concrete buildings containing both surface elements and rebar. IEEE Access, 11:15271–15283.

Xiang, Z., Rashidi, A., and Ou, G. (2021). Automated framework to translate rebar spatial information from gpr into bim. Journal of Construction Engineering and Management, 147(10).